Communication

pubs.acs.org/Biomac

Location of the Bacteriophage P22 Coat Protein C-Terminus Provides Opportunities for the Design of Capsid-Based Materials

Amy Servid,[†] Paul Jordan,[†] Alison O'Neil,[†] Peter Prevelige,[‡] and Trevor Douglas*,[†]

[†]Department of Chemistry and Biochemistry, Montana State University, Bozeman, Montana 59717, United States

[‡]Department of Microbiology, University of Alabama at Birmingham, Birmingham, Alabama, 35294, United States

Supporting Information

ABSTRACT: Rational design of modifications to the interior and exterior surfaces of virus-like particles (VLPs) for future therapeutic and materials applications is based on structural information about the capsid. Existing cryo-electron microscopy-based models suggest that the C-terminus of the bacteriophage P22 coat protein (CP) extends toward the capsid exterior. Our biochemical analysis through genetic manipulations of the C-terminus supports the model where the CP C-terminus is exposed on the exterior of the P22 capsid. Capsids displaying a 6xHis tag appended to the CP C-terminus bind to a Ni affinity column, and the addition of positively or negatively charged coiled coil peptides to the capsid results in association of these capsids upon mixing. Additionally, a single cysteine appended to the CP C-terminus results in the formation of intercapsid disulfide bonds and can serve as a site for chemical modifications. Thus, the C-terminus is a powerful location for multivalent display of peptides that facilitate nanoscale assembly and capsid modification.

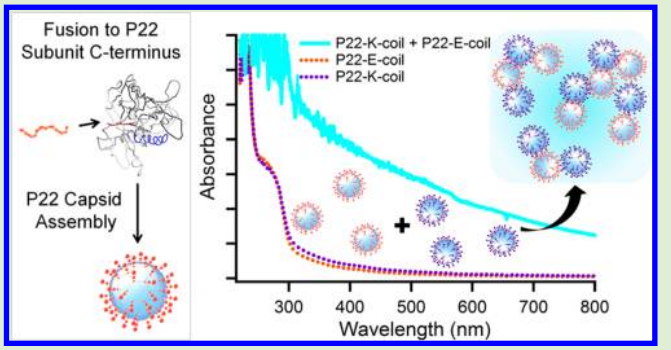

INTRODUCTION

Viruses are increasingly recognized as useful templates for both hard and soft materials applications.[1−3] The multifunctional, and highly symmetric organization of subunits in the viral capsids provide for a unique environment for functional group display and modification.[4,5] Knowledge about the structure and assembly of virus capsids aids their use as powerful platforms for functional nanomaterials design and synthesis.[6−12] The assembly of repeating subunits into capsids generates highly monodisperse multivalent nanoparticles with distinct interior and exterior surfaces that can be used for encapsulation and/or display.[13,14] Encapsulated cargo is sequestered from the surrounding environment, while modifications on the capsid exterior display functionalities that interact directly with the bulk environment.

The capsid derived from the bacteriophage P22 is a robust nanocontainer that has been extensively used for directed encapsulation[15] and surface display,[16] and its use as a biomaterial is completely decoupled from the infectious virus. The noninfectious P22 procapsid (PC) assembles in vivo (in *Escherichia coli*) from 420 copies of coat protein with the aid of the P22 scaffold protein (SP),[17] which can be truncated to include only residues 141−303 and still template assembly of a $T = 7$ virus like particle.[18] The truncated SP (SP141) is packaged on the interior of the 60 nm diameter procapsid and by fusing cargo proteins to the N-terminus can act as a means to direct the packaging inside the P22 capsid.[19] Previously, we have genetically engineered cysteine residues into the P22 coat protein on the interior (S39C, K118C)[20,21] and exterior (T183C)[16] of the assembled P22 capsid to utilize as sites for chemical conjugation.

For the surface display of peptides, a genetic fusion approach is advantageous over chemical conjugation because the stoichiometry of the peptide display is defined by the quaternary structure, and the capsid self-assembles in vivo requiring less processing and a more homogeneous end product. One flexible loop on the capsid exterior has been identified as a potential site for the display of short peptides but does not tolerate large inserts or highly charged peptides.[16] The availability of another, more robust, site for genetic display on the capsid exterior would expand the versatility and application of the P22 nanoplatform. The available models of the P22 capsid (from cryo-TEM)[22,23] suggest that the C-terminal residues of the CP extend toward the exterior of the capsid. However, the models do not include the location of the last few residues of the P22 CP.

Here we have investigated the location of the CP C-terminus in the P22 procapsid by genetically engineering fusion peptides to the C-terminal of the CP and investigating the biochemical presentation of peptides to the exterior environment of the capsid. Natural and synthetic systems utilize coiled coil motifs[24−30] to promote hierarchical assembly, so we have explored the presentation of coiled coil peptides on the C-terminus for directed interparticle interactions. Through these

Received: June 1, 2013
Revised: August 16, 2013

   dx.doi.org/10.1021/bm400796c | *Biomacromolecules* XXXX, XXX, XXX−XXX

studies, we show that fusions to the C-terminus of the P22 CP do indeed sample the exterior environment, and we demonstrate the utility of this approach for display of peptides that allow manipulation of the biophysical properties of the capsid and suggest further development of the P22 platform as a functional nanomaterial.

MATERIALS AND METHODS

Generation of P22 Structural Images. The cryo EM reconstruction coordinates were obtained from the protein data bank (PDB) entries for the procapsid coat protein (PDB: 2XYY), the expanded shell (virion coat protein, PDB: 2XYZ, and P22 expanded head coat protein, PDB: 3IYI), and the wiffleball morphology (PDB: 3IYH). Images were created using UCSF Chimera (version 1.6.2) from the Resource for Biocomputing, Visualization,and Informatics at the University of California, San Francisco.[31]

Expression Vectors. For expression of wtP22/wtSP particles, the previously described assembler plasmid[32] that contains genes corresponding to wt scaffold, wt coat protein, and ampicillin resistance was used. The genes for the novel mCherry capsids presented were generated using a previously described pET $11a^+$ template containing mCherrySP141, K118C CP, and ampicillin resistance.[19] From 5′ to 3′, the mCherrySP141 DNA sequence in the template vector coded for mCherry fluorescent protein, a thrombin proteolytic site, a cysteine (SP-C140), and SP141−303 all in a single reading frame. Established polymerase chain reaction protocols[33] using the C118K, SP-C140A, and CP-431C primers (Figure S1, Supporting Information) were followed to change or add codons in the template. The C118K primer changes a previously described CP variant (K118C) back to wtCP, the SP-C140A substitutes an alanine for the cysteine to create mCherrySP141(C140A), and the CP-431C adds a cysteine to the CP C-terminus (CP-431C).

Genes for the CP C-terminal additions were ligated into the Novagen pRSFDuet-1 (Kan^R) vector to allow for expression of P22 virus-like particles. The coat protein (CP) from the Bacteriophage P22 and a truncated form of the P22 scaffold protein SP(141-303), hereafter referred to as SP141, were incorporated into each of the two multiple cloning sites. Initially, the gene corresponding to the SP141 was amplified from the assembler plasmid[19] and ligated into the first multiple cloning site BamHI and SacI. Ligation into this location yields a 6xHis tag present in the expression vector reading frame directly upstream of the SP141 gene.

Subsequently, the gene for the CP-6xHis was amplified out of the assembler plasmid,[32] and was inserted into the second multiple cloning site of this vector using BglII and XhoI. An SpeI site incorporated upstream of the 6xHis sequence to allow for the insertion of K-coil and E-coil sequences at this site. The primer used for the amplification is shown in Figure S1. K-coil and E-coil flanked by SpeI and XhoI were purchased in a pUC57-Kan vector from Genscript, isolated and ligated downstream of the coat protein gene. Novagen pRSFDuet-1 vectors containing a gene for kanamycin resistance, a truncated P22 scaffold protein (6xHis-SP141), and a P22 coat protein (CP-6xHis, CP-K-coil, or CP-E-coil) were transformed into *E. coli* strain XL1 electro-competent cells (Agilent Technologies). Colonies resulting from each ligation were screened for CP amplification by colony PCR. Isolated plasmids from positive colonies were sequenced (Seqwright, Tx) for verification.

Capsid Expression and Purification. Expression vectors for wtP22/wtSP, wtP22/mCherrySP141, wtP22/mCherrySP141-(C140A), CP-431C/mCherrySP141(C140A), wtP22/6xHis-SP141, CP-6xHis/6xHis-SP141, CP-E-Coil/6xHis-SP141, and CP-K-Coil/6xHis-SP141 P22 capsids were transformed into electrocompentant *E. coli* strain BL21 (DE3, Novagen). One milliliter from an overnight culture was used to inoculate 1 L of Luria broth (LB) supplemented with the appropriate antibiotic (ampicillicin or kanamycin). Cells were grown at 37 °C, and induced with 1 mM isopropyl β-D-1-thiogalactopyranoside (IPTG) at an OD_{600} of 0.6. Approximately 4 h later, cells were collected by centrifugation and lysed with DNase, lysosyme, and RNase (Sigma Aldrich). Sonication was used to disrupt the cells (3× for 2.5 min at 50% amplitude, pulse 0.5 s on/off, Branson Digital Sonifier 250, 200 W, 20 kHz). Large cellular debris were removed through centrifugation (45 min at 12 000*g*). Subsequently, P22 capsids were pelleted through a 35% sucrose cushion for 50 min at 45 000*g* using ultracentrifugation (Sorval WX Ultra 80, Thermo Scientific). Pellets were resuspended in phosphate buffered saline (10−30 mg/mL, pH 7.6), and dialyzed to remove excess sucrose. Size exclusion chromatography (SEC) using a Sephacryl-500 column was completed as a final purification step using phosphate buffered saline (pH 7.6). The P22 capsid concentration was determined with the absorbance at 280 nm using an extinction coefficient A280 = 1.4$(mg/mL)^{-1}$.

Liquid Chromatography−Mass Spectroscopy (LC-MS). Masses of the P22 coat proteins prior to and after modification were determined by using a micro-TOF (Bruker Daltonics) mass spectrometer. Aproximately 1.5 μg (2−4 μL volume) of each P22 sample in phosphate buffered saline (PBS) buffer (25 mM phosphate, 50 mM NaCl, pH 7.6, purified as described previously) was injected via an Agilent 1100 series high-performance liquid chromatography (HPLC) system equipped with a PolyHydroxyethyl A sizing column (100 × 4.6 mm, 5 μm, 500 Å from PolyLC, Inc.). Samples were continuously flowed to the electrospray ionization (ESI) source from the HPLC using an isocratic elution (25% acetonitrile, 75% water, and 0.1% formic acid) and a flow rate of 0.3 $mL\text{-}min^{-1}$. Source parameters were as follows: drying gas 6.0 $L\text{-}min^{-1}$, nebulizer 3.5 bar, capillary voltage 3500 V, capillary exit 100 V. Spectra were collected in positive mode from 200 to 3000 m/z at a rate of 2 Hz. The resulting multiple charge state distributions for protein were deconvoluted using a maximum entropy deconvolution algorithm in the Bruker Compass Analysis software.

Nickel−Nitrilotriacetic Acid (Ni-NTA) Affinity Chromatography. To test for binding of the capsids with 6xHis tags, approximately 0.5 mg (1 mL vol) of each sample was applied to a 1 mL Ni HisTrap column (Pharmacia) equilibrated in PBS. Bound capsids were eluted from the column at a flow rate of 0.5 $mLmin^{-1}$ with a buffer gradient containing 0 to 1 M imidazole in 25 mM HEPES, 100 mM NaCl, pH 7.1. Protein elution was monitored via the absorbance at 280 nm, and fractions containing protein were analyzed by sodium dodecyl sulfate polyacrylamide gel electrophoresis (SDS-PAGE).

SDS-PAGE and Western Blot Analysis. Samples were mixed with 4x loading buffer containing dithiothreitol (DTT) and heated in a boiling water bath for 10 min prior to loading on tris-glycine gels with a 4% polyacrylamide stacking gel and a 15% polyacrylamide running gel (stock solutions made from: Biorad 30% acrylamide/bis solution 29:1, ammonium persulfate, tetramethylethylenediamine (TEMED), and tris(hydroxymethyl)aminomethane (TRIS) base from Fisher). Gels were run at a constant current of 35 mA for approximately 1 h. Upon completion, either gels were stained with coomassie and imaged with a UVP MultDoc-IT Digital Imaging System, or proteins were transferred (2 h at 200 mA) to a Hybond C nitrocellulose membrane (Amersham Biosciences) for Western blot analysis. Nitrocellulose membranes were incubated in blocking solution (5% milk powder in tris-buffered saline with 0.01% Tween-20) overnight at 4 °C, followed by incubation with a 1:2000 dilution of anti-6xHis epitope tagged antibody in blocking solution for 3 h at room temperature. Subsequently, a 1:10 000 dilution of antimouse HRPO conjugate in blocking solution was added for 30 min at room temperature. The membrane was washed with Tris buffered saline (TBS), 0.01% Tween 20 prior to each incubation step, and an Opti-4CN kit (Biorad) was used for detection.

Enzyme Linked Immunosorbent Assay (ELISA). A 1:10 dilution of a commercially available mouse anti-6xHis tag antibody was made into a 50 mM Carbonate buffer, pH 9.6. Fifty microliters of this antibody solution was loaded into each well on a coated 96-well ELISA plate (Nunc) and incubated for approximately 2.5 h at 37 °C. A PBS control containing no protein and each P22 capsid sample at 0.5 mg/mL were diluted 10-fold into buffer (containing 25 mM phosphate, 50 mM NaCl, 0.05% Tween 20, 2% w/v polyvinylpyrrolidone (MW 40 000), 0.2% w/v bovine serum albumin, and 0.02%

dx.doi.org/10.1021/bm400796c | *Biomacromolecules* XXXX, XXX, XXX−XXX

sodium azide), 150 μL was added to each well, and the plate was incubated overnight at 4 °C. The plate was subsequently incubated for 3 h at room temperature with a rabbit antibody recognizing the P22 coat protein in the same buffer used for the capsid incubation. One hundred microliters of antirabbit horseradish peroxidase (HRP) conjugate (Biorad, 1:3,000 fold dilution in 25 mM phosphate, 50 mM NaCl, 0.05% Tween 20, 2% w/v polyvinylpyrrolidone (M_w 40,000), 0.2% w/v bovine serum albumin) was added to each well and incubated at room temperature for 1 h. The plate was washed 5× with PBS, 0.05% Tween 20 after each incubation step. The presence of P22 capsids was detected with a OptEIA ELISA TMB Substrate Reagent Set (BD Biosciences), and the relative absorbance at 350 nm was recorded using a Spectra Max Plus 384 plate reader (Molecular Devices) with a SoftMax Pro 5.4.4 software package. A background absorbance value for the PBS control was subtracted from the each average recorded absorbance to yield the data presented in Figure 2C.

Size Exclusion Chromatography Coupled to Multi-Angle Light Scattering (SEC-MALS). Separation on a size exclusion column (Wyatt Technologies, WTC-0200S) preceded detection using a Wyatt HELEOS multi angle laser light scattering (MALLS) detector, equipped with a quasi-elastic light scattering detector (QELS) and an Optilab rEX differential refractometer (Wyatt Technology Corporation). Twenty five microliters of each capsid at approximately 1.5 mg/mL was injected through the SEC column on an Agilent 1200 HPLC with buffer (50 mM phosphate, 100 mM NaCl buffer, 3 mM sodium azide) at a flow rate of 0.7 mL/min. Astra 5.3.14 software from Wyatt Technology Corporation was used to calculate the number average molecular weight (M_n) from the molecular weight distribution.

Reaction of P22 Cysteines with Fluorescein-5-Maleimide (F5M). Fluorescein-5-Maleimide (Pierce) was reacted with 2 mg (3.1 mg/mL) of each of the following: wtP22/mCherrySP141, wtP22/mCherrySP141(C140A), and CP+431C/mCherrySP141(C140A) procapsid. A 20-fold molar excess of F5M per P22 subunit was added dropwise from a stock solution in dimethyl sulfoxide (DMSO), and the reaction was stirred vigerously for 2 h at room temperature. Pelleting of the procapsids through a sucrose cushion, followed by resuspension and an additional pelleting by ultracentrifugation in PBS buffer removed excess F5M from the samples. Unmodified and labeled samples were diluted 20× into denaturing buffer (6 M Guanidine HCl, 50 mM Phosphate, 100 mM NaCl at pH 7.7), mixed, and UV−visible spectra of the denatured protein samples were recorded approximately 10 min later. The UV−visible absorbance of a series of F5M concentrations in the denaturing buffer was measured to calculate the extinction coefficient of the F5M in these conditions.

Reaction of P22 Cysteines with *N*-Ethyl Maleimide. N-ethylmaleimide (NEM, Pierce) was reacted with P22 capsids to block intercapsid disulfide formation. From a stock solution of 50 mg/mL NEM dissolved in dimethylformamide (DMF), a 50-fold molar excess of NEM per P22 subunit was added dropwise to 2 mg (0.5 mg mL^{-1}) of each wtP22/mCherrySP141(C140A) and CP+431C/mCherrySP141(C140A) capsids in PBS pH 7.0. Controls for the labeling experiments were carried out by the addition of a corresponding volume of neat DMF. After stirring rapidly for 3 h at room temperature, P22 capsids were diluted into pH 7.0 PBS buffer, mixed for 1 h at 4 °C, and pelleted through a 35% sucrose cushion in the ultracentrifuge (50 min at 45 000*g*) to remove unreacted NEM. Samples were subsequently resuspended and pelleted (50 min at 45 000*g*) a second time in pH 7.3 PBS buffer, and left rocking in PBS pH 7.3 overnight at 4 °C. Samples of resuspended protein were analyzed from the supernatant solution after a 5 min centrifugation step at 17 000*g*. Subsequently, 20 uL of DTT stock solution was added to reduce disulfides, resulting in a final concentration of 5 mM DTT, and samples were left to resuspend overnight at 4 °C. Samples of resuspended protein were again analyzed from the supernatant solution after a 5 min centrifugation step at 17 000*g*.

Quartz Crystal Microbalance with Dissipation (QCM-D). CP-K-coil and CP-E-Coil capsids were injected onto gold-coated quartz crystal (Q-Sense, QSX301) positioned in a Q-Sense D300 (Q-Sense AB) quartz crystal microbalance with dissipation. Additions of 600 μL of each sample (CP-K-coil or CP-E-coil) at a concentration of 3.3 μg/mL in 50 mM phosphate, 100 mM NaCl, pH 7.0, were loaded onto the crystal and allowed to equilibrate for 20 min at 25 °C. A 20 min buffer equilibration step at 25 °C followed each capsid addition. The frequency and dissipation values were recorded using the QSoft 301 software program (version 1.6.16.69) interfaced to the instrument.

RESULTS

To probe the location of the structurally unresolved C-terminus of the CP in the bacteriophage P22 capsid, a series of genetic mutations were made and biochemically characterized. In the structural model of the P22 procapsid coat protein, the last five amino acids are not resolved, and their location is ambiguous (Figure 1). However, the published models of the P22 capsid[22,23] suggest that the C-terminus of the CP is directed toward the exterior of the capsid (Figure S2).

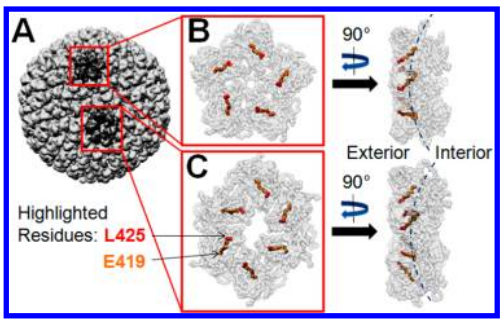

Figure 1. A representation of the assembled P22 procapsid (A) from the published cyroEM structure, which includes residues 1−425 of the 430 amino acid P22 coat protein. The residues 419−425 are highlighted in the zoomed versions of the pentamer (B) and hexamer (C) units. In both, it appears that the CP C-terminus extends toward the capsid exterior.

Genetic fusion of short peptides to the C-terminus of the CP was used to test the accessibility of this region to the exterior environment of the P22 procapsid. A 6x-histidine tag, a single cysteine residue, and two coiled coil peptides, were individually fused to the CP C-terminus to create the following new P22 coat protein constructs: CP-431C, CP-6xHis, CP-E-coil, and CP-K-coil. The genetic manipulation was confirmed by DNA sequencing. Each of the four new P22 coat proteins (CP-6xHis, CP-431C, CP-E-coil, and CP-K-coil) were individually coexpressed with a P22 SP to facilitate the self-assembly of the procapsids in the *E. coli* expression system. The novel procapsids were purified using the same methodology as used for purification of the wtP22 procapsids,[19] which included ultracentrifugation through a sucrose cushion, followed by SEC (Sephacryl S-500, Figure S3). Analysis of these materials by SDS page gel electrophoresis confirms the presence of both P22 coat protein and scaffold protein (Figure S4).

No significant changes in particle assembly were observed upon the addition of amino acids to the C-terminus. The addition of the residues to the CP C-terminus, on the purified P22 constructs, was confirmed by LC-MS analysis (Figures S5 and S6). By SEC, all constructs eluted at approximately 65 mL, which is consistent with the elution volume of the assembled wtP22 procapsid (Figure S3). The fractions from this peak were pooled and subjected to HPLC-SEC coupled to multiangle light scattering (MALS) and refractive index detection. Analysis of the light scattering revealed packaged procapsids with particle diameters reflecting that of assembled capsids for each sample (Figure S7) and all of the capsids had particle RMS radii

dx.doi.org/10.1021/bm400796c | *Biomacromolecules* XXXX, XXX, XXX−XXX

in the 23−30 nm range and hydrodynamic radii between 25 and 33 nm. The mass of each procapsid calculated from multiangle light scattering was observed to be between 22 and 30 MDa. (Figure S7) The radii and mass ranges reflect slight differences in the construct size and packaging of cargo; each individual construct is highly monodisperse (Figure S7).

To determine whether the coat protein 6xHis tag is exposed on the capsid exterior, three different variants of the P22 procapsid were studied. These P22 variants included CP with C-terminal 6xHis tag combined with a scaffolding protein having a N-terminal 6xHis tag, a wild-type CP combined with a scaffolding protein having a N-terminal 6xHis tag, and a wild type CP combined with a wild type scaffold protein (CP-6xHis/6xHis-SP141, wtCP/6xHis-SP141, and wtCP/wtSP, respectively). In each case, the scaffold protein is packaged on the interior of the P22 procapsid. The exposure of the CP-6xHis tag to the exterior of the capsids was probed by binding to a Ni chelate affinity column. The only construct that demonstrated binding to the Ni column was the CP-6xHis/6xHis-SP141, and these capsids could be eluted by an increasing imidazole gradient (Figure 2A). In contrast, the

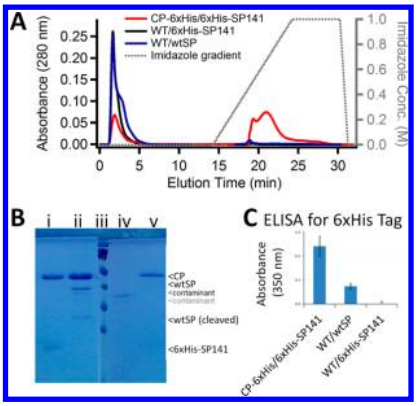

Figure 2. Nickel chromatography and ELISA assays with assembled P22 procapsid to determine the exposure of 6xHis tags to the capsid exterior. (A) Elution chromatograms of CP-6xHis/6xHis-SP141, wtCP/6xHis-SP141, and wtCP/wtSP from a Ni HisTrap column with increasing imidazole concentration. (B) SDS-PAGE analysis of peaks in affinity chromatogram A: (i) 2 min elution peak: wtCP/6xHis-SP141, (ii) 2 min elution peak: wtCP/wtSP, (iii) Page Ruler Molecular Weight standard, (iv) 2 min elution peak: CP-6xHis/6xHis-SP141, and (v) 21 min elution peak: CP-6xHis/6xHis-SP141. (C) Enzyme Linked Immunabsorbent Assay displaying the relative amount of each assembled P22 capsid that interacts with an anti-His antibody.

wtCP/6xHis-SP141 and wtCP/wtSP samples did not bind to the column (Figure 2A). The presence of P22 VLPs in all fractions was confirmed by SDS-PAGE gel (Figure 2B). The CP-6xHis/6xHis-SP141 sample exhibited a peak at 2 mL corresponding to protein that did not bind to the column. Analysis of this peak by SDS-PAGE indicates both the absence of P22 CP-6xHis/6xHis-SP141 and the presence of a protein contaminant (Figure 2Biv) that appears on an SDS-PAGE gel of the sample prior to affinity chromatography (Figure S8). The binding of CP-6xHis/6xHis-SP141 but not wtCP/6xHis-SP141 to the Ni column is a clear indication that the 6xHis tag on the CP is presented to the exterior of the P22 capsid. The lack of binding by the wtCP/6xHis-SP141 construct also strongly suggests that the scaffold protein is sequestered on the interior and does not sample the outside to any significant extent.

Additional data supporting the exposure of the CP-6xHis on the exterior of the procapsid was obtained via an ELISA sandwich assay utilizing a 6xHis tag antibody and a CP specific antibody. A 96-well plate was coated with anti-His tag antibody and each well was subsequently incubated with CP-6xHis/6xHis-SP141, wtCP/6xHis-SP141, or wtCP/wtSP capsids. The binding of each P22 construct to the anti-His antibody was probed by the CP antibody (rabbit) and subsequently quantified by a secondary goat-antirabbit antibody via a HRP/TMB colorimetric assay.[34] The highest absorbance was observed for the CP-6xHis/6xHis-SP141 construct, while the wtCP/6xHis-SP141 was similar to the background measurement of the assay (Figure 2C).

A Western blot confirmed that the 6xHis tags were present on 6xHis-SP141, and that they could be recognized by the same anti-His antibody used in the ELISA (Figure S8) but only after capsid denaturation. The coat and scaffold proteins were separated by SDS-PAGE and transferred to a nitrocellulose membrane, which was incubated with the mouse anti-His antibody. Bands containing 6xHis tags were subsequently detected using a rabbit-antimouse HRP conjugated secondary antibody. Bands corresponding to 6xHis tags on the coat and scaffold were both detectable, while neither the wtCP nor wtSP were highlighted (Figure S8). Together, these data are consistent with the suggestion from the structural models and with binding of this construct to the Ni column, indicating that peptides fused to the CP C-terminus are accessible to the capsid exterior while the scaffolding protein is sequestered on the capsid interior. Demonstrating the display of the CP-6xHis on the capsid exterior provides the foundation for future utilization of the CP C-terminal location for the display of targeting peptides or antigenic epitopes.

To further investigate the accessibility of the C-terminus to the capsid exterior, a single cysteine was appended to the C-terminus of the CP (CP-431C/mCherrySP141(C140A)). The addition of a single cysteine residue is less likely to cause alterations in the procapsid structure than longer charged peptides. Successive quick change mutagenesis steps were carried out on a previously described vector,[19] resulting in the creation of two unique P22 constructs (wtCP/mCherrySP141 and wtCP/mCherrySP141(C140A), in route to obtaining CP-431C/mCherrySP141(C140A).

To demonstrate the utility of both the C-terminal CP-431C and scaffold protein cysteine (SP-C140) as a sites for chemical conjugation, wtCP/mCherrySP141, wtCP/mCherrySP141-(C140A), and CP-431C/mCherrySP141(C140A) were each reacted with fluorescein-5-maleimide (F5M). The F5M labeling of each capsid was quantified by monitoring the UV−visible absorbance of unmodified and F5M reacted capsids under denaturing conditions (Figure S9), after separation of free F5M from the capsids by ultracentrifugation through a sucrose cushion. Calculations indicated that F5M labeling resulted in 176 F5M per wtCP/mCherrySP141 capsid and 272 F5M per CP-431C/mCherrySP141(C140A), while only 40 F5M per capsid were observed for the wtCP/mCherrySP141(C140A) capsid (Figure S9). LC-MS confirmed the labeling of CP-431C with F5M, while no F5M labeling of the CP was observed for the wtCP/mCherrySP141 or wtCP/mCherrySP141(C140A)-(Figure S10). These data demonstrate the cysteine packaged inside the wtCP/mCherrySP141 is a useful site for chemical conjugation, and the utility of the procapsid CP C-terminal cysteine chemical conjugation with imaging agents.

dx.doi.org/10.1021/bm400796c | *Biomacromolecules* XXXX, XXX, XXX−XXX

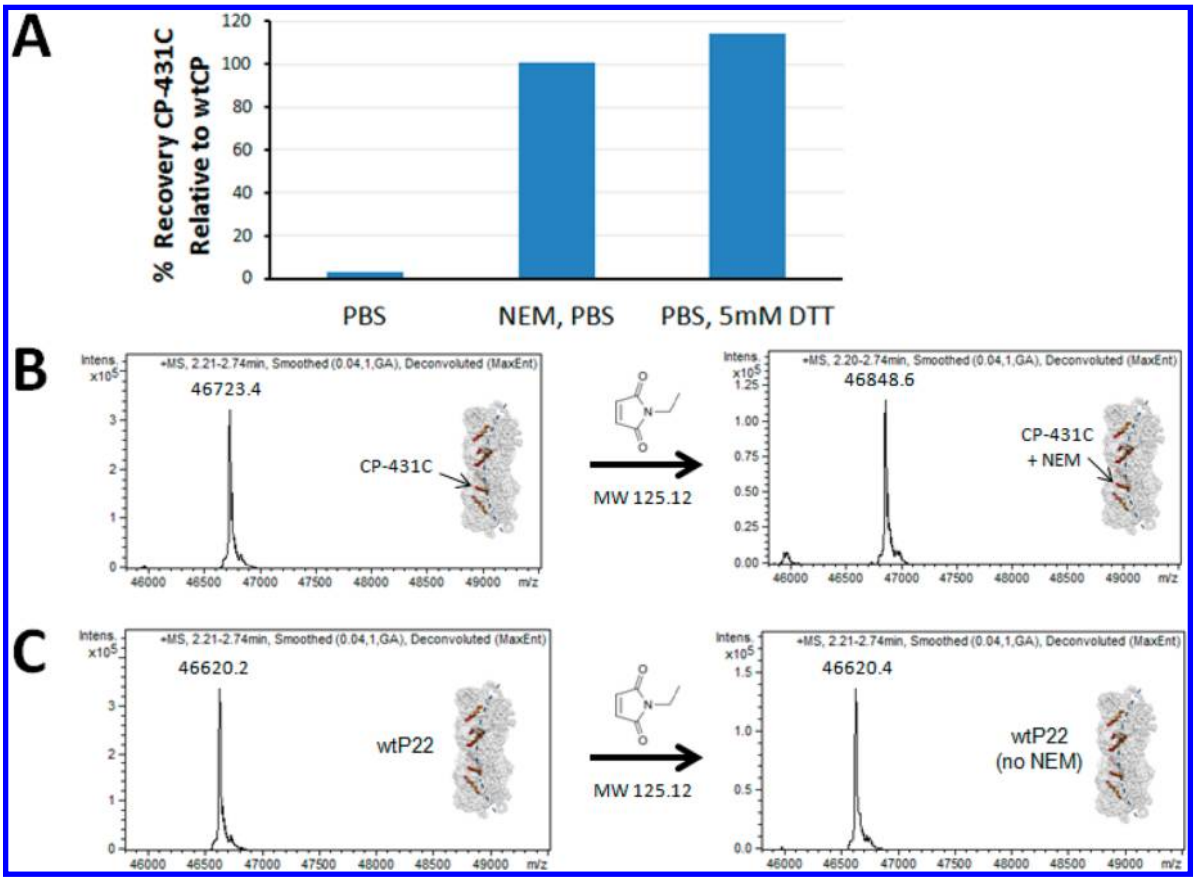

Figure 3. Evidence for disulfide bond formation between CP-431C/mCherrySP141(C140A) capsids. (A) Bar graph showing the relative yield of soluble CP-431C/mCherrySP141(C140A) protein compared to wtCP/mCherrySP141(C140A) after resuspension in PBS buffer, PBS buffer after blocking CP-431C/mCherrySP141(C140A) with NEM and in PBS buffer and with 5 mM DTT. (B) Mass spectrum of CP-431C/mCherrySP141(C140A) before and after labeling with NEM. (C) Mass spectrum of wtCP/mCherrySP141(C140A) before and after labeling with NEM. The original m/z data is shown in Figures S5 and S6.

In an effort to further confirm the labeling of the wtCP/mCherrySP141, the mass spectroscopy data was analyzed. Under the chromatography and ionization conditions utilized, the P22 CP ionizes much more efficiently than mCherrySP141 or mCherrySP141(C140A). This results in very poor signal intensity and resolution for the peaks at corresponding to the mCherrySP141 (with a predicted mass of 45962 Da) and mCherrySP141(C140A) (with a predicted mass of 45994 Da) (Figure S10). Therefore, any labeling of the scaffold protein could easily be in the baseline noise of the spectrum.

We probed the formation of disulfide bonds in this construct to investigate the ability of the single CP C-terminal cysteine to protrude to the exterior of the capsid, and result in the formation of intercapsid interactions. SEC purified CP-431C/mCherrySP141(C140A) was pelleted by ultracentrifugation and it was observed that, in contrast to the wtCP/mCherrySP141(C140A), this construct did not readily resuspend when incubated at 4 °C overnight. Since the fluorescent protein mCherry is packaged on the capsid interior, the difference in the sample behavior was easily observed qualitatively by eye (Figure S11), and a comparison of the yield of resupended protein was quantified by UV−visible spectroscopy (Figure S11). Relative to the wtCP/mCherrySP141-(C140A), only 3% of CP-431C/mCherrySP141(C140A) was recovered (Figure 3A).

To confirm that disulfide bond formation played a role in the inefficient resuspension of the CP-431C/mCherrySP141-(C140A) construct, the capsid was treated with N-ethyl maleimide to block cysteine thiols. Labeling of the CP subunits was confirmed via liquid chromatography mass spectroscopy analysis, in which all CP subunits were observed to be modified for the CP-431C/mCherrySP141(C140A) construct (Figure 3B), while the wtCP/mCherrySP141(C140A) showed no labeling under the same reaction conditions (Figure 3C). Excess NEM was purified from the capsids via ultracentrifugation through a sucrose cushion, and SEC-MALS analysis revealed that the morphology of the capsids was retained after labeling (Figure S7). Upon pelleting of the NEM-labeled CP-431C/mCherrySP141(C140A), the capsid resuspended in PBS buffer with a recovery identical to wtCP/mCherrySP141(C140A) under these conditions (Figure 3A). This is supporting evidence for the creation of an intercapsid network from exposed cysteines in CP-431C/mCherrySP141-(C140A).

Having evidence for disulfide formation between capsids, we hypothesized that recovery of the CP-431C/mCherrySP141-(C140A) construct might be accomplished through the addition of a reducing agent. Upon addition of DTT (5 mM), the CP-431C/mCherrySP141(C140A) construct resuspended with an apparent 114% recovery compared to wt capsid under the same conditions (Figure 3A and Figure S11). Dynamic light scattering measurements indicated the presence of intact procapsids (average radius of hydration, R_h= 58.6 ± 0.3 nm for wtCP/mCherrySP141(C140A); R_h= 59.3 ± 1.6 nm

dx.doi.org/10.1021/bm400796c | *Biomacromolecules* XXXX, XXX, XXX−XXX

for CP-431C/mCherrySP141(C140A)) under these reducing conditions for both wtCP/mCherrySP141(C140A) and CP-431C/mCherrySP141(C140A) capsids (Figure S12). This provides additional evidence for the existence of disulfide association between CP-431C/mCherrySP141(C140A) capsids.

Building on our demonstrations that peptide extensions to the CP C-terminus are displayed on the capsid exterior and can mediate interparticle interaction, we explored coiled coil motifs to direct interparticle association and assembly. Coiled coil peptides can be described as heptad repeats of amino acids that form superhelical structural motifs when mixed. Strong associations between peptides arise from packing of hydrophobic residues at the interface between the helices and stabilization of the supercoiled structure through electrostatic interactions.

A pair of antiparallel heterodimeric coiled coil petides was used to transform individual P22 procapsids into building blocks for an extended network structure. Amino acid sequences corresponding to either a positive (CP-K-coil, +TR$(VAALKEK)_3$) or negatively charged (CP-E-coil, +TS-$(VAALEKE)_3$) α helix of a three heptad heterodimeric coiled coil motif were appended to the C-terminus of the coat protein. Peptide sequences, $VAALKEK_3$ and $VAALEKE_3$, have been previously described to form a antiparallel coiled coil heterodimer upon association.[25] The genetic amenability of the C-terminal location is reflected in the addition of these 23 residues without noticeable alterations to the assembly of the P22 procapsid.

The inherent multivalent interactions between the shorter three heptad-coiled coils on each capsid promote significant capsid interactions, despite having a less thermally stable heterodimer than longer heptad coiled coil repeats.[35] We used the three-heptad system in an effort to avoid kinetic traps in material assembly, which are less probable in the particle–particle assembly based upon the cumulative effect of many weak interactions. Upon mixing of solutions containing 0.5 mg/mL of the CP-E-coil and CP-K-coil capsids, a significant increase in light scattering was observed within seconds (Figure 4A), indicating interaction and association of capsids within this mixture to form larger particulates. No increase in scattering was observed with control samples containing each of CP-E-coil or CP-K-coil individually, or the mixture of each coil construct with wtP22 capsid (Figure 4A). Single spectra of the CP-E-coil and CP-K-coil capsids at 1 mg/mL individually, and after mixing are shown in Figure S13.

The capacity of the coiled coil interaction between the C-termini of adjacent procapsids to facilitate assembly on a surface, using a layer-by-layer approach, was monitored via quartz crystal microbalance with dissipation (QCM-D). The CP-K-coil (20 μg) was deposited on a gold-coated quartz sensor followed by a buffer wash and equilibration and subsequent addition of CP-E-coil (20 μg) and another buffer equilibration. This process was repeated two more times in the layer-by-layer deposition process (Figure 4B). Each addition of P22 resulted in a decrease in frequency (Δf) indicating deposition of the protein on the crystal surface and was also accompanied by an increase in the dissipation (D) at each step.

CONCLUSIONS

Here we have shown that the C-terminal region of the coat protein from the bacteriophage P22 is indeed exposed to the exterior environment of the capsid. From the available cryo-electron microscopy models, the exact location of the C-terminus of the CP is slightly ambiguous. Using genetic manipulation of the C-terminus, including the addition of a single cysteine residue to the C-terminus, incorporation of a 6xHis motif, and genetic fusion of complementary coiled-coil peptides, we have established that these modifications to the C-terminus are exposed to the exterior of the capsid. This greatly enhances the ability to use the P22 capsid system as a functional nanomaterial and we have demonstrated this unique site on the capsid can be used for small molecule chemical conjugation, as well as for fabrication of capsid-based extended materials through the directed interparticle interaction mediated by disulfide bond formation and directed coiled-coil interactions.

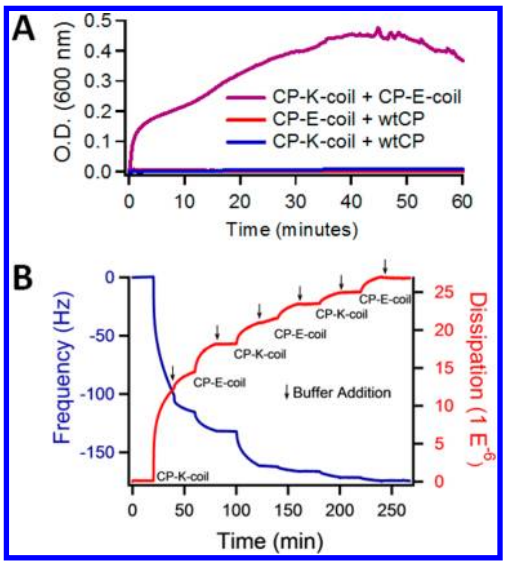

Figure 4. Interaction of P22 procapsids displaying K-coil (+TR-$(VAALKEK)_3$) or E-coil (+TR$(VAALEKE)_3$) peptides appended to the CP c-terminus. (A) UV–visible spectroscopy showing an increase in scattering upon mixing of the E-coil and K-coil capsids relative to each capsid individually or mixtures with wtP22. (B) Assembly of K-coil and E-coil capsids on a surface was observed via quartz crystal microbalance with dissipation.

ASSOCIATED CONTENT

Supporting Information

Additional results are available in the Supporting Information. This material is available free of charge via the Internet at http://pubs.acs.org.

AUTHOR INFORMATION

Corresponding Author

*E-mail: tdouglas@chemistry.montana.edu; phone: (406) 994-6566.

Notes

The authors declare no competing financial interest.

ACKNOWLEDGMENTS

The authors wish to thank Rui Li for the anti-CP antibody used in the ELISA and Western Blots, Dustin Patterson for helpful discussions about the assembly of materials via coiled coil interactions, and Ravi Kant for assistance with the QCM-D instrumentation. This work was supported in part by grants from the National Institutes of Health, NIBIB R01-EB012027 (design and construction of the C-terminal constructs), and the

U.S. Department of Energy, Office of Basic Energy Sciences, Division of Materials Science and Engineering, DE-FG02-07ER46477 (hierarchical assembly of E-coil and K-coil constructs).

REFERENCES

(1) Chen, C.; Daniel, M. C.; Quinkert, Z. T.; De, M.; Stein, B.; Bowman, V. D.; Chipman, P. R.; Rotello, V. M.; Kao, C. C.; Dragnea, B. *Nano Lett.* **2006**, *6*, 611−615.
(2) Ma, Y. J.; Nolte, R. J. M.; Cornelissen, J. *Adv. Drug Delivery Rev.* **2012**, *64*, 811−825.
(3) de la Rica, R.; Matsui, H. *Chem. Soc. Rev.* **2010**, *39*, 3499−3509.
(4) Carrico, I. S.; Kirshenbaurn, K. *Nat. Nanotechnol.* **2009**, *4*, 14−15.
(5) Kirshenbaum, K.; Zuckermann, R. N.; Dill, K. A. *Curr. Opin. Struct. Biol.* **1999**, *9*, 530−535.
(6) Aniagyei, S. E.; Kennedy, C. J.; Stein, B.; Willits, D. A.; Douglas, T.; Young, M. J.; De, M.; Rotello, V. M.; Srisathiyanarayanan, D.; Kao, C. C. *Nano Lett.* **2009**, *9*, 393.
(7) Huang, Y.; Chiang, C.-Y.; Lee, S. K.; Gao, Y.; Hu, E. L.; Yoreo, J. D.; Belcher, A. M. *Nano Lett.* **2005**, *5*, 1429−1434.
(8) Royston, E.; Ghosh, A.; Kofinas, P.; Harris, M. T.; Culver, J. N. *Langmuir* **2008**, *24*, 906−912.
(9) Stephanopoulos, N.; Liu, M.; Tong, G. J.; Li, Z.; Liu, Y.; Yan, H.; Francis, M. B. *Nano Lett.* **2010**, *10*, 2714−2720.
(10) Wang, Q.; Lin, T.; Johnson, J. E.; Finn, M. *Chem. Biol.* **2002**, *9*, 813−819.
(11) Yoo, P. J.; Zacharia, N. S.; Doh, J.; Nam, K. T.; Belcher, A. M.; Hammond, P. T. *ACS Nano* **2008**, *2*, 561−571.
(12) Kostiainen, M. A.; Hiekkataipale, P.; Jose, Á.; Nolte, R. J.; Cornelissen, J. J. *J. Mater. Chem.* **2011**, *21*, 2112−2117.
(13) Uchida, M.; Klem, M. T.; Allen, M.; Suci, P.; Flenniken, M.; Gillitzer, E.; Varpness, Z.; Liepold, L. O.; Young, M.; Douglas, T. *Adv. Mater.* **2007**, *19*, 1025−1042.
(14) Capehart, S. L.; Coyle, M. P.; Glasgow, J. E.; Francis, M. B. *J. Am. Chem. Soc.* **2013**, *135*, 3011−3016.
(15) Patterson, D. P.; Prevelige, P. E.; Douglas, T. *ACS Nano* **2012**, *6*, 5000−5009.
(16) Kang, S.; Lander, G. C.; Johnson, J. E.; Prevelige, P. E. *ChemBioChem* **2008**, *9*, 514−518.
(17) Earnshaw, W.; Casjens, S.; Harrison, S. C. *J. Mol. Biol.* **1976**, *104*, 387−410.
(18) Parker, M. H.; Casjens, S.; Prevelige, P. E. *J. Mol. Biol.* **1998**, *281*, 69−79.
(19) O'Neil, A.; Reichhardt, C.; Johnson, B.; Prevelige, P. E.; Douglas, T. *Angew. Chem., Int. Ed.* **2011**, *50*, 7425−7428.
(20) Lucon, J.; Qazi, S.; Uchida, M.; Bedwell, G. J.; Lafrance, B.; Prevelige, P. E., Jr.; Douglas, T. *Nat. Chem.* **2012**, *4*, 781−8.
(21) Kang, S.; Uchida, M.; O'Neil, A.; Li, R.; Prevelige, P. E.; Douglas, T. *Biomacromolecules* **2010**, *11*, 2804−2809.
(22) Chen, D. H.; Baker, M. L.; Hryc, C. F.; DiMaio, F.; Jakana, J.; Wu, W. M.; Dougherty, M.; Haase-Pettingell, C.; Schmid, M. F.; Jiang, W.; Baker, D.; King, J. A.; Chiu, W. *Proc. Natl. Acad. Sci. U.S.A.* **2011**, *108*, 1355−1360.
(23) Parent, K. N.; Sinkovits, R. S.; Suhanovsky, M. M.; Teschke, C. M.; Egelman, E. H.; Baker, T. S. *Phys. Biol.* **2010**, *7*, 045004.
(24) Altunbas, A.; Pochan, D. J. *Peptide-Based Materials*; Deming, T., Ed.; Springer: Berlin Heidelberg, 2012; pp 135−167.
(25) Pechar, M.; Pola, R.; Laga, R.; Ulbrich, K.; Bednarova, L.; Malon, P.; Sieglova, I.; Kral, V.; Fabry, M.; Vanek, O. *Biomacromolecules* **2011**, *12*, 3645−3655.
(26) Minten, I. J.; Nolte, R. J. M.; Cornelissen, J. *Macromol. Biosci.* **2010**, *10*, 539−545.
(27) Patterson, D. P.; Desai, A. M.; Holl, M. M. B.; Marsh, E. N. G. *RSC Adv.* **2011**, *1*, 1004−1012.
(28) Kopecek, J.; Yang, J. Y. *Angew. Chem., Int. Ed.* **2012**, *51*, 7396−7417.
(29) Fletcher, J. M.; Harniman, R. L.; Barnes, F. R.; Boyle, A. L.; Collins, A.; Mantell, J.; Sharp, T. H.; Antognozzi, M.; Booth, P. J.; Linden, N.; Miles, M. J.; Sessions, R. B.; Verkade, P.; Woolfson, D. N. *Science* **2013**, *340*, 595−599.
(30) Apostolovic, B.; Danial, M.; Klok, H. -A. *Chem. Soc. Rev.* **2010**, *39*, 3541−3575.
(31) Pettersen, E. F.; Goddard, T. D.; Huang, C. C.; Couch, G. S.; Greenblatt, D. M.; Meng, E. C.; Ferrin, T. E. *J. Comput. Chem.* **2004**, *25*, 1605−1612.
(32) Prevelige, P. E., Jr; Thomas, D.; King, J. *J. Mol. Biol.* **1988**, *202*, 743−757.
(33) Kirsch, R. D.; Joly, E. *Nucleic Acids Res.* **1998**, *26*, 1848−1850.
(34) Frey, A.; Meckelein, B.; Externest, D.; Schmidt, M. A. *J. Immunol. Methods* **2000**, *233*, 47−56.
(35) Pechar, M.; Pola, R. *Biotechnol. Adv.* **2013**, *31*, 90−96.